Available online at www.sciencedirect.com
ScienceDirect
ELSEVIER
February 2016, 23(1): 73–85
www.sciencedirect.com/science/journal/10058885
The Journal of China Universities of Posts and Telecommunications
http://jcupt.bupt.edu.cn

Real-time dynamic system to path tracking and collision avoidance for redundant robotic arms

Gao Xin (✉), Jia Qingxuan, Sun Hanxu, Chen Gang, Zhang Qianru, Yang Yukun

School of Automation, Beijing University of Posts and Telecommunications, Beijing 100876, China

Abstract

An dynamic system for real-time obstacle avoidance path planning of redundant robots is constructed in this paper. Firstly, the inter-frame difference method is used to identify the moving target and to calculate the target area, then on the basis of color features and gradient features extracted from the target area, the feature fusion Cam-Shift mean shift algorithm is used to track target, improving the robustness of the tracking algorithm. Secondly, a parallel two-channel target identification and location method based on binocular vision is proposed, updating the target's three-dimensional information in real time. Then, a dynamic collision-free path planning method is implemented: the safety rods are removed through the intersection test, and the minimum distance is derived directly by using the coordinate values of the target in the local coordinate system of the rod. On this basis, the obstacle avoidance gain and escape velocity related to the minimum distance is established, and obstacle avoidance path planning is implemented by using the zero space mapping matrix of redundant robot. Experiments are performed to study the efficiency of the proposed system.

Keywords redundant robots, identification and tracking of moving target, three-dimensional positioning, dynamic obstacle avoidance path planning

1 Introduction

With the continuous expansion of the application scope for robots, it is difficult for robots of low degree freedom to complete some complex manipulation tasks [1]. But for redundant robots, the freedom degrees of the joints' are greater than the freedom degrees that the end pose defines, so within the joint space each of the joints can move from an initial position to a desired position of the joint while keeping the end actuator pose unchanged. Because of this characteristic, the redundant robots overcome some shortcomings of general robots, such as poor flexibility, low obstacle avoidance ability, joints overrun and poor dynamic performance and etc [2–5].

An important technology of the redundant robot applications is obstacle avoidance path planning. The effective collision-free planning method can reduce a lot of operating time, protecting the robot from damaging; at the same time, it can save manpower and capital investment, laying a good foundation in more areas for robots application [6–7]. The robot dynamic obstacle avoidance path planning means, the robot itself is moving, obstacle moves too, and the end of the robot reaches the destination not touching any moving obstacle. In unknown dynamic environment, redundant robot must have the ability to perceive the environment and to move to the destination independently, and the uncertainty of obstacles has greatly increased the complexity of the task.

Currently, there are many studies on obstacle avoidance path planning [8–10]. The free-space method was proposed by Lazona-Perze [6]. The method solved the entire C space, achieving free space and obstacle space, but it required to build C space for dynamic obstacles online, which would take a lot of time, and can't meet the real-time requirements. The artificial potential fields approach, a unique obstacle avoidance approach, was used to allow real time multi-joint robots operations in a complex environment [11]. Most of the potential functions approach will help in the robot navigation, however the

Received date: 29-09-2015
Corresponding author: Gao Xin, E-mail: xlhhh74@bupt.edu.cn
DOI: 10.1016/S1005-8885(16)60011-0

local minima problem remained. Another widely used method was the gradient projection method (GPM) proposed by Liegeois [9]. Although GPM just was a local solution comparing to global optimization schemes, it was more computationally effective and more suitable for real-time implementation. However, one of the biggest problems associated with GPM was how to select an appropriate scalar coefficient. Oriolo et al. [12] proposed a method for real-time map building and navigation for a mobile robot, where a global path planning plus a local graph search algorithm and several cost functions were used. Tian et al. used the genetic algorithm to search collision-free trajectories for two degrees of freedom manipulator [13]. Regarding the minimum of joint displacement as optimization goal, they realized the obstacle avoidance path planning within the global scope. However, with the increase in the degree of freedom, the heuristic search algorithm costed large amount of calculation time, which is not suitable for real-time obstacle avoidance planning for redundant manipulators.

Some neural-network models [14–17] were proposed to generate real-time robot trajectories through learning. Zalama et al. [16] proposed a neural-network model for a mobile robot navigation, which can generate dynamic collision-free trajectories through unsupervised learning. This model was computationally complicated since it incorporated the vector-associative-map model and the direction-to-rotation effector control transform model. Sugie et al. presented a method which achieves autonomous obstacle avoidance with rate constraints [18]. Furthermore, this method was applied to an actual two-link robot manipulator and its effectiveness was evaluated by experiment. Jasour et al. presented a nonlinear model predictive control (NMPC) for redundant robotic arms [19]. Using NMPC, the end-effector of robotic arm tracked a predefined geometry path in the Cartesian space in such a way that no collision with obstacles in the workspace and no singular configurations for robot occurs. But this kind of control method establishing the nonlinear model costed large amount of calculation time and was not applicable to dynamic planning.

This paper presents an efficient dynamic system for real-time obstacle avoidance path planning of redundant robots. First of all, the inter-frame difference method is used to identify the moving target and to calculate the target area, then on the basis of color features and gradient features extracted from the target area, the feature fusion Cam-Shift mean shift algorithm is used to track target; secondly, a two-channel parallel target identification and location method based on binocular vision is proposed, updating the target three-dimensional information in real time while tracking it; then, considering the real-time characteristics of obstacle avoidance path planning for redundant robots, a dynamic collision-free path planning method is implemented: the safety rods are removed through the intersection test, and the minimum distance is derived directly by using the coordinate values of the target in the local coordinate system of the rod. On this basis, the obstacle avoidance gain and escape velocity related to the minimum distance is established, and obstacle avoidance path planning is implemented by using the zero space mapping matrix of redundant robot. Experiments are performed to study the efficiency of the proposed system.

2 System architecture

The system structure of dynamic obstacle avoidance path planning based on binocular vision for redundant robot is shown in Fig. 1. The whole system consists of the part of computer vision and that of redundant robot dynamic obstacle avoidance path planning. Three-dimensional information of the moving object obtained by computer visual processing is passed to the obstacle avoidance module of redundant robot to implement dynamic obstacle avoidance path planning.

The function of computer vision module is as follows: firstly, the binocular camera is used to get the redundant robot environment information, and then the obtained video sequences are preprocessed by hue-saturation-value (HSV) space threshold dividing, median filtering, connected component labeling and morphological processing and etc. On this basis, the computer vision portion is divided into two parallel channels: one channel, the inter-frame difference method is used to detect dynamic target and mark the target area; while the color characteristic value, the gradient feature value and the edge feature point of the object are extracted in the region. Improved Cam shift search algorithm is used to track the moving target and draw its trajectory. Another channel, the edge feature points of the object are used for stereo matching, and the average three-dimensional coordinates of the feature points are determined by using parallax information; finally, three-dimensional information of moving targets is updated in real time while tracking it.

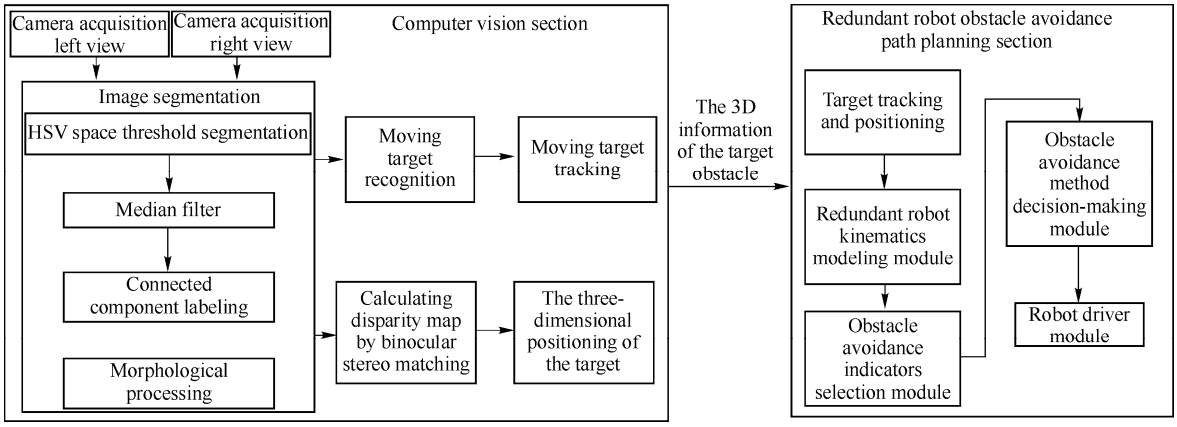

Fig. 1 Overall block diagram of the dynamic obstacle avoidance system for redundant robot

The part of dynamic obstacle avoidance path planning for redundant robot is divided into four modules: kinematics equations construction module, obstacle avoidance indicators selection module, the decision-making module of obstacle avoidance method and robot driver module. Firstly, kinematics and inverse kinematics model of redundant robot is established, and the position relationship between the obstacle and redundant robot bars is judged according to the pre-selected the minimum distance indicators. Then escape velocity dynamic obstacle avoidance method is chosen in decision-making module of obstacle avoidance, and the zero-space mapping matrix of redundant robot is used to complete obstacle avoidance task, finally drive each joint of the robot to move.

3 Identification and tracking methods of moving target

The article discusses the moving target identification under the conditions of the fixed camera and in a static background. The moving target detection and extraction methods in a static background mainly include the inter-frame difference algorithm, background subtraction algorithm and optical flow estimation algorithm [20]. On the basis of the analysis, considering quickly identify requirement, the inter-frame difference method is chosen to identify moving target and calculate the target area. Then moving target tracking algorithms are researched in-depth. Mean-shift algorithm is insensitive to the moving target pose changes and calculates quickly. However, the mean shift Cam Shift algorithm is only based on color feature, and when the color feature of target is not obvious or color values of objects in the background are similar to the target, Cam Shift algorithm will track failure [21], so the optimized multi-feature fusion method is used, and the color and gradient features of target are extracted to make up for the lack of single feature, which improves the robustness of the dynamic target tracking.

3.1 Moving target recognition and area calculation

Adjacent frame difference method is simple and easy to be implemented, so it is suitable to be used for real-time moving target detection [22]. Because the time interval of the adjacent frame is generally very short, the algorithm is less sensitive to light changes of the scene, and effect of the target shadow is also relatively small, which make it has better adaptability to the dynamic environment. In moving target identification test, the monocular camera is used to capture the rose red object moved by experimenter's hand, and the adjacent frame difference method is used to recognize the moving target and calculate the target area, as shown in Fig. 2. Fig. 2(a) is the first frame image of the target video sequences, (b) is the second frame image, (c) is a binarization result which minus two adjacent images. Through the area threshold processing and morphological filtering, the moving target is identified, as shown in Fig. 2(d).

(a) First frame image (b) Second frame image

(c) Binarized image (d) Identification the target

Fig. 2 Identification and area determination process of moving target

As can be seen from the above, the identification result of the adjacent frame difference method is ideal when the target moves slowly, and its operation is simple, which meets the real-time requirements during the recognition process. Meanwhile it is less affected due to changed ambient illumination condition. But the target region identified is lightly larger than that of the real object.

3.2 Cam shift tracking method based on moving target feature fusion

Traditional Cam Shift method only extracts the color characteristics of the target area for moving target tracking [21], and the visual image of the target is with a variety of features, such as color model features, gradient model features, contour feature, frequency domain characteristics and etc. Each feature model has its own applicability, and color characteristics can easily lead to the failure of target tracking when target color is similar to background color. The gradient characteristic of the target is with a certain amount of space configuration information, and can compensate for the defects. Therefore, a fusion feature model of color and gradient features is used in this paper, which combines the advantages of color histogram and gradient histogram features to improve the robustness of the Cam Shift tracking algorithm, laying a good foundation for dynamic obstacle avoidance path planning later.

1) Color Histogram

The HSV color space model divides the color signal into three properties respectively, hue, saturation and brightness. With respect to the red-green-blue (RGB) model, the HSV color model is more consistent with the human visual judgment [23]. But under normal circumstances the RGB model is obtained directly from the images and needs to be transformed. Generally, in order to strengthen the robustness of histogram expression, the kernel function of spatial information is added to calculate weighted histogram, which gives the pixels that the distance is near from the center of the target the greater weights, but the pixels that the distance is far from the center the smaller weights.

2) Gradient histogram

Although the color histogram is a wide used model, it hides the space location information of the image, and it is easy to be affected by changes in the external environment, such as light et.al. Therefore, in order to track the moving target better in real-time, the concept of gradient histogram is introduced. Firstly, chrominance image of the target image is calculated, and then to calculate the gradient magnitude and the direction of all the pixels within the chrominance picture. A variety of image gradient methods mainly depend on the selection of the calculated points, and four neighborhood field calculation method is used in this paper.

3) The Fusion of the Target Feature

As the color and gradient histograms are used, the fusion of the target feature is calculated as follows:

$$\omega = \frac{1}{2\pi\delta_{\mathrm{c}}\delta_{\mathrm{g}}}\exp\left[-\frac{1}{2}\left(\alpha\frac{d^2_{\mathrm{color}}}{\delta^2_{\mathrm{c}}}+\beta\frac{d^2_{\mathrm{grad}}}{\delta^2_{\mathrm{g}}}\right)\right] \tag{1}$$

where, δ_{c} and δ_{g} represent the noise variance of the color histogram and the gradient histogram respectively, and α, β is used to adjust the weighted value of the two. In addition, the target tracking is often affected by external conditions in a complex environment, such as the state mutation of the tracking object, obscured target and light et.al. If the histogram template is constant, it can't effectively deal with these changes, and the template update strategy should be used, as shown in the following formula:

$$p_{\mathrm{u},k} = (1-\eta)p_{\mathrm{u},k-1} + \eta q_{\mathrm{u},k-1} \tag{2}$$

where, $q_{\mathrm{u},k-1}$ is the optimum matching area for target, $p_{u,k-1}$ is a histogram template of the current frame, η is the scale factor.

In order to verify the effectiveness of the tracking algorithm, under the conditions of computer Pentium dual-core CPU, 2.50 GHz frequency, the memory 2 GB, video images are captured by a monocular camera BNT D881 (200 million pixels, the maximum resolution of 1 200 × 1 600 dots/inch, maximum frame rate 30 frame/s). Firstly in the case that target is integrity and is not deformed, color of objects in the background is similar to the target object, traditional Cam shift algorithm is used

for moving target tracking, and the experimental results are shown in Fig. 3.

(a) The 10th frame

(b) The 15th frame

(c) The 20th frame

Fig. 3 Tracking performance of traditional Cam shift algorithm in the similar color background

Figs. 3(a) and (b) is 10th and 15th tracking image in the video sequences respectively. In the 10th, the tracking results are satisfactory, and the target area extracted is accurate; while the distance between the target object and the green background gradually decreases, the target area began to shake in the 15th, and there is a tendency of the offset. In the 20th, as shown in Fig. 3(c), when the green object is adjacent to greenery in the background, the traditional Cam shift method only using color feature also judges green plant as a tracking target, resulting in serious deviation of the target area.

Multi-feature extraction method, integration of the color histogram and gradient histogram, is used to implement the target tracking, and Fig. 4 is the effect diagram by using proposed method. Figs. 4(a) and (b) is 10th and 18th tracking image in the video sequences respectively. Tracking effect is ideal, and the target region is extracted accurately. While the green target is close to the green plants on the background, as shown in the following diagram (c), this method is still able to accurately track the target, and the tracking effect does not be affected.

(a) The 10th frame

(b) The 18th frame

(c) The 26th frame

Fig. 4 Tracking performance of optimized Cam shift algorithm in the similar color background

4 Three-dimensional positioning method of target

This paper presents a binocular visual target identification and location method based on edge features and parallax information, which is divided into two parallel channels, as shown in the Fig. 5.

4.1 Uniform edge feature points extraction of target recognition region

Detection results of Canny edge detection operator is closer to the intuitive results, and it can be combined with the dynamic obstacle avoidance bounding box, so the Canny operator is used to extract edge features [24]. Canny edge detection algorithm is improved in the paper, the achieved window of target recognition is set as the edge detection area, that is, only the image within the recognition window is detected, reducing detection information of the computer image processing. Following figure is the experiment results comparison. The original picture is shown in Fig. 6(a), which the moving target is a rose red small ball. The Fig. 6(b) shows the edge detection of the whole picture, and it can be seen that Canny operator extracts the information of all edges. Fig. 7 shows edge detection only for objects within the target area. Fig. 7(a) shows the target area is extracted by the adjacent frame difference method, and the coordinate values of the target area in the current frame are stored, and then only to detect edge information for objects within the target area using Canny operator, as shown in the Fig. 7(b) below.

The goal of stereo matching is to get the three-dimensional coordinates of the center of the sphere in the world coordinate system, and the first thing that comes to mind is the extraction and matching of the center of the sphere. But the segmentation results are vulnerable to the impact of light, and the image coordinates of the center extracted are only approximate coordinates, which will cause large errors and lead to the large amount of calculation. According to the needs of dynamic obstacle

avoidance and spherical characteristics, the feature points on the spherical edge are obtained, and then the average values of feature points are calculated to get the coordinates of sphere center. Taking into account the large number of edge feature points, the average extraction method of edge feature points is used.

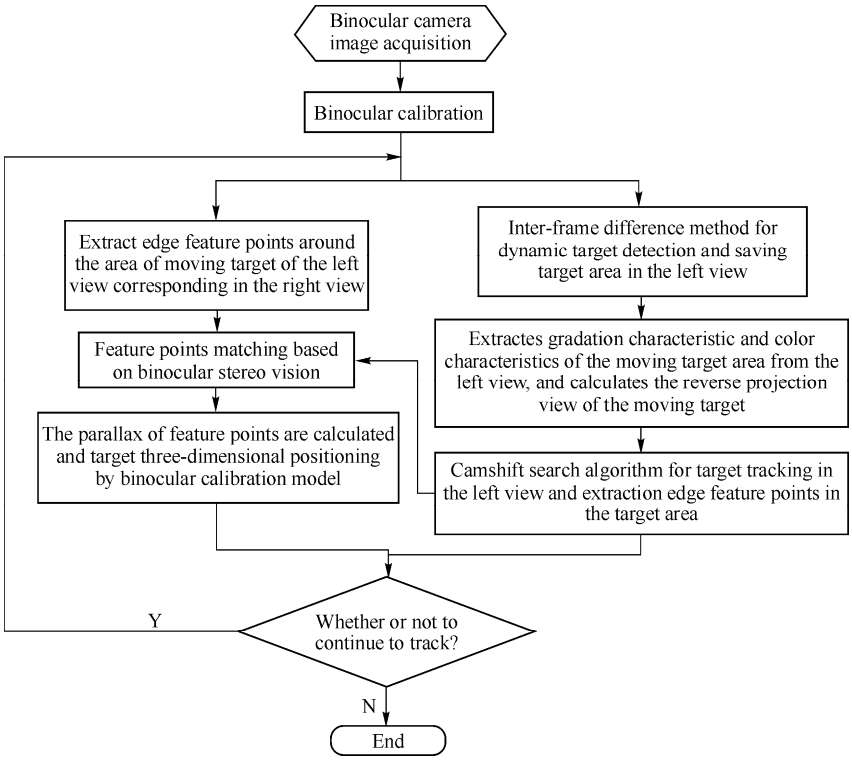

Fig. 5 Overall flow chart of binocular visual target identification and positioning method based on edge features and parallax information

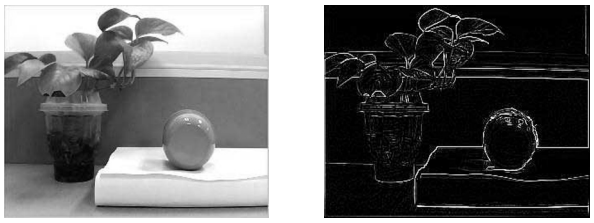

(a) Original picture (b) Edge detection

Fig. 6 Canny edge detection

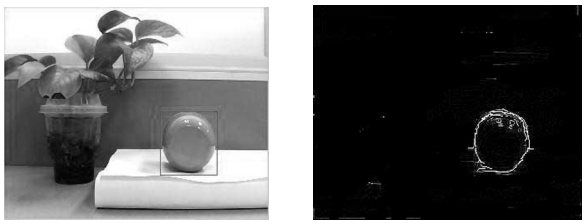

(a) Extracting the target (b) Edge detection within the target area

Fig. 7 Edge detection for objects within the target area

The idea in detail is as follows: eight feature points extracted on the left spherical edge are used to match at right view, each point forty-five degrees apart, so we can get eight pairs of matching points. It is very difficult to achieve the uniform extraction for the eight points during the process of the actual operation, mainly because the coordinates extracted is not an integer, and the edge discontinuity etc. So, the following method is used to extract the edge points: according to coordinate values of center O and radius R, the approximate pixel coordinates of the circle at the eight points can be obtained. But the edge of the ball is intermittent, the approximate pixel coordinates may not be on the edge points. The approximate pixel coordinates are taken as the center, looking for the detected edge points in the neighborhood, in which an arbitrary point is selected as the matching point.

4.2 Stereo matching of edge feature points

Eight feature points in spherical edge are extracted

according to the above method, and then to find corresponding match points. Assuming the coordinate of one point is $t(x, y)$, the feature point image is calculated firstly, as shown in the following formula.

$$\left.\begin{aligned} t(x,y) &= \min\{H,V,L,R\} \\ H &= [f(x,y)-f(x-1,y)]^2+[f(x,y)-f(x+1,y)]^2 \\ V &= [f(x,y)-f(x,y-1)]^2+[f(x,y)-f(x,y+1)]^2 \\ L &= [f(x,y)-f(x-1,y+1)]^2+[f(x,y)-f(x+1,y-1)]^2 \\ R &= [f(x,y)-f(x+1,y+1)]^2+[f(x,y)-f(x-1,y-1)]^2 \end{aligned}\right\} \tag{3}$$

where, H, V, L and R are calculated with the gray gradient. Now considering the stereo matching for the image pairs composed of the left and right images. For each feature point of the left image, a possible match collection can be obtained, which is composed of all possible matching points in the right image. So a label set for each feature point of the left image can be obtained, wherein the index may be the parallax of the feature point of the left image and its possible matching point, or represent a special label for no match point. For each possible match point, the initial match probability $P^{(0)}(l)$ is set by the following formula.

$$A(l) = \sum_{(x,y)\in W}\left[f_L(x,y)-f_R(x+l_x,y+l_y)\right]^2 \tag{4}$$

where, $l=(l_x,l_y)$ is represented as possible parallax. $A(l)$ is the gray fit goodness between the two regions, which is inversely proportional with the initial matching probability $P^{(0)}(l)$. In other words, $P^{(0)}(l)$ is related to the similarity of possible match points neighborhood. Accordingly, the relaxation iterative method can be taken to give a positive incremental for the parallax relatively close points within possible match neighborhood, and to give a negative incremental for the parallax relatively far points, iterative updating of $P^{(0)}(l)$. With the iterative calculation, the kth matching probability $P^{(0)}(l)$ of correctly matched points will gradually increase, and the $P^{(0)}(l)$ of the other points will gradually reduce. After a certain number of iterations, the point with the maximum matching probability $P^{(0)}(l)$ is determined as the match point. Finally, the normalized grayscale cross-correlation function is used to look for the matching points, and the window size is $(2n+1)\times(2m+1)$, which m, n is a positive integer, taking $m=n=2$. The definition of the function is as shown in the following Eq. (5):

$$C(x,y,x',y') = \frac{\sum_{i=-n}^{i=n}\sum_{i=-m}^{i=m}\left[I(x+i,y+j)-\overline{I(x,y)}\right]\left[I'(x'+i,y'+j)-\overline{I'(x',y')}\right]}{\sqrt{\left[\sum_{i=-n}^{i=n}\sum_{j=-m}^{j=m}\left(I(x+i,y+j)-\overline{I(x,y)}\right)^2\right]\left[\sum_{i=-n}^{i=n}\sum_{j=-m}^{j=m}\left(I'(x'+i,y'+j)-\overline{I'(x',y')}\right)^2\right]}} \tag{5}$$

where, $\overline{I(x,y)}=\sum_{i=-n}^{i=n}\sum_{i=-m}^{i=m}I(x+i,y+j)\Big/\left[(2n+1)\times(2m+1)\right]$, $\overline{I'(x',y')}=\sum_{i=-n}^{i=n}\sum_{i=-m}^{i=m}I'(x'+i,y'+j)\Big/\left[(2n+1)\times(2m+1)\right]$. $\overline{I(x,y)}$ represents the average gray value of the pixels within the rectangular window $(2n+1)\times(2m+1)$ and the (x,y) as the center in the left image, and $\overline{I'(x',y')}$ represents the same principle. The point (x',y') with the largest correlation value $C(x,y,x',y')$ is the matching point of point (x,y). The effect for extracting feature points on the target sphere is shown in Fig. 8, and the effect for point-to-point stereo matching using normalized algorithm is shown in Fig. 9.

Fig. 8 Uniform edge feature point extraction

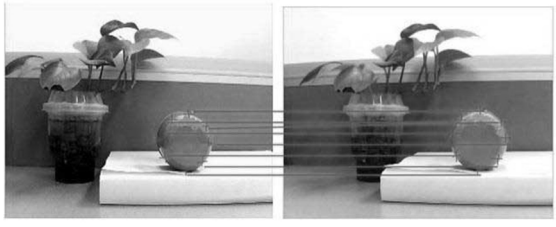

Fig. 9 Stereo matching for feature points

To illustrate the validity of the target identification and location method based on the edge feature and binocular disparity information, a parallel alignment configuration

binocular stereo visual system is built for the experiment, taking the coordinate system of left camera as the world coordinate system. The depth information extraction steps are as follows:

1) To build parallel alignment configuration binocular stereo vision system. Two cameras (the BNT D881) are placed parallel strictly, the distance in accordance with the baseline B = 13 cw, focal length f = 15 mm, and ensuring a consistent high degree.

2) Camera Calibration. The two cameras are calibrated to obtain internal and external parameters by the Zhang's two-step method respectively [25].

3) The two images of the measured moving objects are obtained by the binocular cameras, and adjacent frame difference method is used to identify the moving target, and to extract the target area.

4) The edge characteristics of the object will be extracted in the target area. First, the image is dealed with gray scale processing, and then the Canny operator is used to make edge detection for the area of the moving sphere, and eight edge feature points are uniform extracted.

5) The point-to-point matching algorithm is used to obtain eight pairs of edge matching feature points, and a disparity map is obtained.

6) Depth information extraction and calculation. According to the obtained disparity map and the internal and external parameters of calibration camera, depth information is extracted using the triangulation principle, and then to calculate the average value of eight pairs of edge feature points, that is, the coordinates of the sphere center and the depth information of the sphere center relative to the left camera. Experimental results of the target three-dimensional positioning are shown in the Table 1.

Table 1 Three-dimensional positioning for the target sphere

Test No	x/mm	y/mm	z (Measuring distance)/mm	Actual distance/mm	Error rate/%
1	37.2	32.5	343.9	344.5	1.3
2	28.3	19.5	348.1	348.9	1.6
3	31.8	34.3	450.4	451.6	2.3
4	68.1	112.3	497.1	499.9	2.8
5	121.5	68.3	525.9	528.9	2.3
6	83.4	96.9	554.2	551.1	2.1
7	103.2	110.3	644.1	640.9	2.3
8	115.8	128.5	762.9	768.6	3.4

The experiment results show that error is less than 4%, and meets the positioning accuracy requirements of moving obstacles in the dynamic obstacle avoidance path planning. As can be seen from the Table 1, measurement error also gradually increases with increasing the depth distance of the measured target. This is because the camera used in the experiment has a fixed resolution, and the farther the distance from the camera to the object to be measured, the smaller the imaging of the measured object on the imaging plane, and thus the useful information pixels containing in the imaging is less, leading to reduction in the accuracy of stereo matching and the increase of the relative error.

5 Dynamic obstacle avoidance path planning method for the redundant robot

5.1 Obstacle avoidance indicators

Whether is suitable or not for the selection of obstacle avoidance index will directly affect the effects of obstacle avoidance. Especially for dynamic obstacle avoidance, obstacle moves randomly, and it is very important for real-time obstacle avoidance planning to select the reasonable indicators that can quickly and accurately describe the position relationship between the obstacle and the robot arms.

5.1.1 Pre-select the minimum distance indicators

Traditional distance indicators need to calculate the distance of the obstacle to each rod, then to take the minimum. When the rods are in some special configuration, the minimum distance may fall into the extended line of the rod. Extension line does not belong to the part of the robot, and will lead to inaccurate calculation. So the minimum distance of the traditional distance indicators method is calculated by traversing multiple selected flags in the rod, which has high computational complexity.

Considering the real-time characteristics of collision-free path planning, a pre-selected minimum distance indicators $H_{\text{d-min}}$ is used [26]: the corresponding bounding box for a different configuration of robot is established and the safety bar is removed through the intersection test, and the minimum distance is derived directly by using target coordinate values in the local coordinate system of the rod. If a plurality of rods intersect, $H_{\text{d-min}}$ takes the smallest intersect distance. In the process of obstacle avoidance, the bigger $H_{\text{d-min}}$ is, the better is. The establishing process is shown in the Fig. 10.

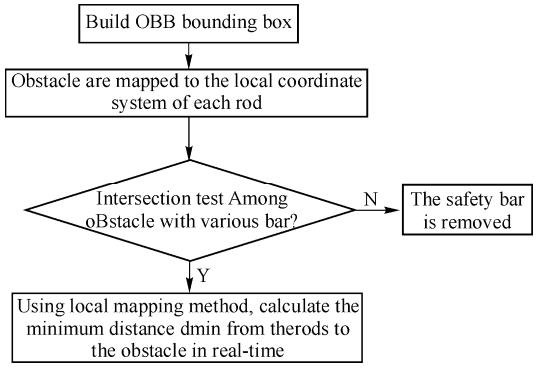

Fig. 10 Establishing process of pre-select the minimum distance obstacle avoidance indicators

5.1.2 Establishment of the bounding box

For redundant robot, especially for the robot that all the joints are rotary joints, the oriented bounding box (OBB) is different from the general bounding box, and its good tightness can adapt to the lever changes of the position and direction, without loss of obstacle avoidance space [27]. Building OBB bounding box just let the direction of the bounding box to be coincided with the direction of the lever, and when the levers rotate, the substrate of the bounding box rotates as well, without the cumbersome conversion direction calculation. The center coordinates of the bounding box are coordinates of the intermediate point of the each lever, the length is the length of the rod; width and height is set to the minimum safety distance d of the robot respectively. The spherical bounding box is used for the different shapes moving obstacles. Assumed that the center coordinates and radius of the sphere is (x_0, y_0, z_0) and R respectively, the equation of the sphere can be described as $(x-x_0)^2+(y-y_0)^2+(z-z_0)^2=R^2$.

5.1.3 Collision detection

The detection method of separation axis is used in the OBB bounding box. Two convex body sets, A and B, are given, and if the two sets have no intersection, it certainly exists a separating hyperplane P, which A and B are located at the sides of the plane. Projection to the straight-line separating axis L, the projection intervals do not overlap. OBB bounding box is up to fifteen separate axis in the base coordinate system, and only all projections in the separation axis overlap in order to determine intersect, which is very tedious. Converting the coordinates of the obstacle to the local coordinate system of each rod, the intersection test is completed in the local coordinate system, and separation axis is reduced to three, namely, the X, Y and Z. Each rod of redundant robot has a corresponding transformation matrix $\boldsymbol{T}$ and the rotation matrix $\boldsymbol{R}$. If c_0 is the coordinates of an obstacle in the base coordinate system, R_{0n} is the rotation matrix of the lever n with respect to the base coordinate system, c_n is the coordinates of the obstacle in the local coordinate system of the rod n, then $c_0 = R_{0n}c_n$, therefore $c_n = R_0^+ c_0$, as shown in Fig. 11.

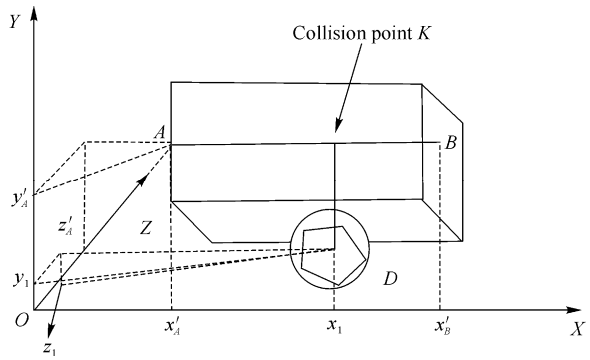

Fig. 11 Intersection tests in the local coordinate system of the lever AB

For lever AB, the coordinates of endpoint A is (x'_A, y'_A, z'_A), and the coordinates of the endpoint B is (x'_B, y'_B, z'_B), the length and width of bounding box is $2d$, height is the same as lever length L; the radius of the sphere is R, the center coordinates is $D_1(x_1, y_1, z_1)$, i.e. $D_1 = R_{01}^+ D_0$, where, D_0 is the center point coordinates of the spheroid in the base coordinate system. The bounding boxes of the lever AB and sphere are projected to the three coordinate axes respectively, and when the three formulas set up at the same time, the lever AB is judged to collide with the obstacles. Otherwise, safety levers need to be removed.

$$\begin{cases} \left|x'_A - x_1\right| \leqslant R + d \\ y'_A - R \leqslant y_1 \leqslant y'_B + R \\ \left|z'_A - z_1\right| \leqslant R + d \end{cases} \tag{6}$$

5.1.4 Local mapping minimum distance calculation

Assuming that lever AB and obstacle intersect, value of the minimum distance $d_{\min}$ is unchanged in arbitrary coordinate system because it is scalar. Calculating collision

point K is in order to obtain the Jacobi matrix J_0 of collision point. $|KA|$, which is also a scalar, is needed when the Jacobian matrix J_0 is calculated by vector product method. So the calculation is implemented directly in the local coordinate system of the rod, no conversion to the base coordinate system, as shown in Fig. 12.

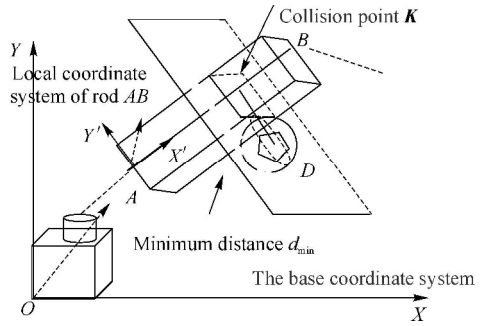

Fig. 12 Minimum distance calculation in the coordinate system of the lever

In the local coordinate system of the lever AB, the coordinates of endpoint A is (x_A', y_A', z_A'), the endpoint B coordinates is (x_B', y_B', z_B'), and the coordinates of obstacle center is $D_1(x_1, y_1, z_1)$. Then the coordinates of collision point K is (x_1, y_A', z_A'); the distance of collision point to rod endpoint A: $\mathrm{KA} = |x_1 - x_A'|$; the minimum distance: $d_{\min} = |y_1 - y_A'|$. Local mapping method for calculating the distance can obtain the outcome directly by using the coordinate values of the target point, eliminating the need for the cumbersome solution of a large number of equations. The use of pre-select the minimum distance indicators $H_{d-\min}$ in dynamic obstacle avoidance saves the intersection detection time, meeting the real-time requirements of the dynamic collision-free path planning.

5.2 Dynamic obstacle avoidance path planning

5.2.1 GPM

GPM [9] is the basic method to solve the inverse kinematics problem of redundant robot, which divides the solution of inverse kinematics into two parts: the minimum norm solution and homogeneous solution, as shown below:

$$\dot{\boldsymbol{q}} = \boldsymbol{J}^{+}\dot{\boldsymbol{x}} + k\left[\boldsymbol{J}_0\left(\boldsymbol{I} - \boldsymbol{J}^{+}\boldsymbol{J}\right)\right]^{+}\nabla H(q) \tag{7}$$

In the above formula, the amplification coefficient k directly affects the speed of self movement of robot, and the larger k is, the greater the optimizing ability be. However, one of the biggest problems associated with GPM is how to select an appropriate scalar coefficient k. If k is too large, it will cause the joint velocity to exceed limits and also result in possible oscillations. If k is too small, it will greatly reduce the optimization capability of the homogenous solution. And what is even worse is, in a continuous trajectory, a given k value is impossibe to be suitable for all configurations. In another words, sooner or later it will always reach an ill condition during the process. Therefore it is necessary to find a method to calculate the optimizing ability for self-motion redundant robot and adjust the amplification factor k online.

5.2.2 Escape velocity dynamic obstacle avoidance path planning

After the minimum distance $d_{\min}$ is calculated, dynamic obstacle avoidance algorithm with escape velocity is used for path planning. The Eq. (7) provides the required joint velocity meeting terminal movement, but if an obstacle exists in the workspace of the robot, one or more connecting rods may be too near away from the obstacle or collide with the obstacle in a state. So, a "threshold" distance should be set, and if the distance of all rods to obstacle is greater than the ‘threshold’ distance, collision-free conditions is met, robot pose obtained by the minimum norm solution will not change. On the contrary, in the case that does not change the position and orientation of the terminal, the robot pose should be adjusted to meet the no obstacle conditions by taking advantage of the zero space vector.

If the rod intersects with an obstacle by the collision detection in a moment, the collision point of the rod and the obstacle is labeled as x_0, and the zero space vector should be selected in order to avoid obstacles for redundant robot, which makes the nearest point have a velocity component $\dot{x}_0$ away from the obstacle, preventing the obstacle from colliding with the lever. Therefore, redundant robot obstacle avoidance path planning should meet the two basic requirements: the first is to meet the requirements of end movement, and the second is to dodge the moving obstacles. That is

$$\boldsymbol{J}\dot{\boldsymbol{q}} = \dot{\boldsymbol{x}} \tag{8}$$

$$\boldsymbol{J}_0\dot{\boldsymbol{q}} = \dot{\boldsymbol{x}}_0 \tag{9}$$

$\dot{x}_0$ is the setting speed to avoid obstacles, and J_0 is the Jacobian matrix of the collision point. Using

self-motion of the redundant robot for obstacle avoidance, the safest obstacle avoidance solution is chosen in the joint zero space, and inverse kinematics formula is expressed as follows:

$$\dot{\boldsymbol{q}} = \boldsymbol{J}^{+}\dot{\boldsymbol{x}} + \left[\boldsymbol{J}_{0}\left(\boldsymbol{I} - \boldsymbol{J}^{+}\boldsymbol{J}\right)\right]^{+}(\dot{\boldsymbol{x}}_{0} - \boldsymbol{J}_{0}\boldsymbol{J}^{+}\dot{\boldsymbol{x}}) \tag{10}$$

In the above formula, $\left[J_0\left(I - J^{+}J\right)\right]^{+}(\dot{x}_0 - J_0 J^{+}\dot{x})$ is called obstacle avoidance items. Because the obstacle moves in real-time, the collision point will change any time, and leads to the rank change of J_0 , which may cause the discontinuous of the joint velocity, and even cause the jitter of the joint. In order to reduce the impact of rank changes, and to maintain the continuity of the joint velocity, the obstacle avoidance gain a_n and escape velocity a_0 are introduced, and the inverse kinematics of the escape velocity dynamic obstacle avoidance is expressed as:

$$\dot{\boldsymbol{q}} = \boldsymbol{J}^{+}\dot{\boldsymbol{x}} + a_{n}\left[\boldsymbol{J}_{0}\left(\boldsymbol{I} - \boldsymbol{J}^{+}\boldsymbol{J}\right)\right]^{+}(a_{0}\dot{\boldsymbol{x}}_{0} - \boldsymbol{J}_{0}\boldsymbol{J}^{+}\dot{\boldsymbol{x}}) \tag{11}$$

where, the speed direction $\dot{x}_0$ is set to the reverse direction of the moving obstacle. The obstacle avoidance gain a_n and the escape velocity a_0 related to the minimum distance are represented as a function of the minimum distance. Three threshold distances are set as d_1, d_2 and d_3.

When $d_{\min} > d_3$, safe area, the distance of obstacles and rods meets collision-free conditions, a_0, a_n are 0, and the robot pose drawn by the pseudo-inverse solution does not need to be changed, that is, the minimum norm solution. The width and height of OBB bounding box are decided by d_3.

When $d_2 < d_{\min} < d_3$, warning area, a_n increases uniformly and obstacle avoidance entry is open, a_0 is equal to 0, the bar can be away from the obstacle without introducing the escape velocity.

When $d_1 < d_{\min} < d_2$, danger area, with the $d_{\min}$ reduction, a_0 increases rapidly. The escape velocity away from obstacle is increased in the connecting rod, and the zero spatial mapping matrix of redundant robot is used for path planning.

When $d_{\min}$ is equal to d_1, the escape velocity reaches the maximum value.

Because the obstacle avoidance gain and escape velocity change smoothly, the joint movement of the robot is continuous during the process of obstacle avoidance, avoiding the occurrence of jitter.

6 Experimental results

In order to verify the validity of the dynamic obstacle avoidance method, this method is applied to nine degrees of freedom modular robot experiment platform. Redundant robots implement the task of grabbing the cup, as shown in Fig. 13. The 9-DOF redundant modular robot includes a mobile joint, the eight rotational joints and the end gripper, wherein the stroke of the moving rail is 3 m, and the spacing of the rail is 1 m. Denavit-Hartenberg method is used to establish the link coordinate system of the robot. The transformation matrix among the various coordinate systems by DH parameters is shown as follows:

$${}_{i}^{i-1}T = \begin{bmatrix} c\theta_i & -s\theta_i & 0 & a_{i-1} \\ s\theta_i c\alpha_{i-1} & c\theta_i c\alpha_{i-1} & -s\alpha_{i-1} & -d_i s\alpha_{i-1} \\ s\theta_i s\alpha_{i-1} & c\theta_i s\alpha_{i-1} & c\alpha_{i-1} & d_i c\alpha_{i-1} \\ 0 & 0 & 0 & 1 \end{bmatrix} \tag{12}$$

where, $c\theta_i = \cos\theta_i$, $s\theta_i = \sin\theta_i$, $1 \leqslant i \leqslant 9$.

Table 2 D-H parameters of 9-DOF robot

i	a_{i-1}	α_{i-1}/(°)	d_i	$\theta_{\min} \leqslant \theta_i \leqslant \theta_{\max}$ /(°)
1	0	0	d_1	0
2	0	− 90	385	$-160 \leqslant \theta_2(0) \leqslant 160$
3	0	− 90	110	$-160 \leqslant \theta_3(0) \leqslant 160$
4	0	90	380	$-160 \leqslant \theta_4(0) \leqslant 160$
5	0	90	0	$-70 \leqslant \theta_5(90) \leqslant 250$
6	135	180	0	$-70 \leqslant \theta_6(90) \leqslant 250$
7	0	90	380	$-250 \leqslant \theta_7(-90) \leqslant 70$
8	0	− 90	0	$-100 \leqslant \theta_8(0) \leqslant 100$
9	0	90	185	$-180 \leqslant \theta_9(0) \leqslant 180$

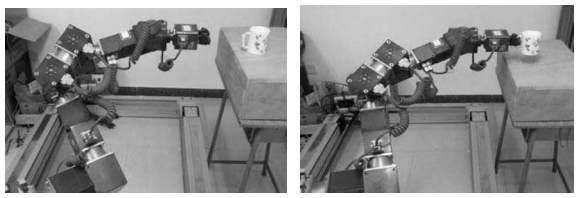

Fig. 13 Task of grabbing cup for the redundant robot

During the process of grabbing cups for the redundant robot, the moving obstacle appears within the

configuration of the robot, as shown in Fig. 14(a). Now the joint angles of redundant robot are (−53.283, −56.254, 70.525, -56.849, 41.237, 82.838, 21.913, −31.629), which are set to the initial value for the robot dynamic obstacle avoidance, and the step size is set to 0.5° per second. The test needs 36s to complete the task. The process of redundant robot dynamic obstacle avoidance is as shown in Fig. 14. The joint angle values of the robot at each second are as shown in Table 3 below.

(a) The 1th second

(b) The 9th second

(c) The 17th second

(d) The 25th second

(e) The 33th second

Fig. 14 The experiment for the redundant robot dynamic obstacle avoidance

Table 3 Robot joint angle change values in 0.5° step size

Time/s	Joint 1/(°)	Joint 2/(°)	Joint 3/(°)	Joint 4/(°)	Joint 5/(°)	Joint 6/(°)	Joint 7/(°)	Joint 8/(°)
1	− 53.283	− 56.254	70.525	− 56.849	41.237	82.838	21.913	− 31.629
3	− 53.014	− 56.012	70.013	− 56.536	40.168	82.136	21.865	− 31.628
5	− 52.865	− 55.389	69.865	− 57.246	39.013	82.010	21.563	− 31.627
7	− 52.846	− 55.125	69.453	− 57.019	37.985	82.003	21.436	− 31.623
9	− 52.523	− 55.569	68.013	− 57.569	36.278	83.596	21.703	− 31.513
11	− 51.863	− 54.893	68.569	− 58.106	35.569	83.463	22.563	− 31.579
13	− 51.012	− 53.968	68.103	− 58.356	34.156	83.296	22.103	− 31.546
15	− 52.856	− 52.457	67.865	− 59.769	33.483	83.043	22.569	− 31.549
17	− 52.014	− 51.021	67.130	− 59.983	32.109	82.867	22.725	− 31.601
19	− 51.956	− 50.039	68.045	− 59.960	31.257	82.596	22.065	− 31.603
21	− 51.106	− 50.239	68.596	− 58.826	30.426	82.289	21.826	− 31.953
23	− 52.569	− 49.453	69.134	− 58.713	29.159	82.183	21.752	− 31.914
25	− 52.689	− 48.395	69.796	− 58.426	27.989	83.079	21.603	− 31.883
27	− 52.946	− 49.128	70.240	− 58.256	28.156	83.004	21.156	− 31.872
29	− 53.453	− 50.453	70.683	− 57.996	29.753	83.005	21.004	− 31.705
31	− 53.689	− 51.569	70.702	− 57.856	30.359	82.865	21.001	− 31.790
33	− 53.017	− 52.896	70.906	− 57.436	31.456	82.469	21.556	− 31.689
35	− 52.893	− 53.012	71.516	− 57.130	32.289	82.286	21.856	− 31.617

In the above experiment, because the moving obstacle is near the module joint 5, the joint 2 and the joint 5 change significantly. The change of the joint 5 mainly makes the robot to escape from obstacle along the reverse movement direction of the obstacle, and the change of joint 2 mainly controls the robot to lift lever in the vertical direction so as to bypass the moving obstacle. Finally, the robot successfully avoids the moving obstacle while completing the task of grabbing the cup.

7 Conclusions and future work

In this paper, the problem of obstacle avoidance path planning for redundant robots in unknown dynamic environment was studied. A real-time dynamic system to path tracking and collision avoidance for redundant robotic arms was proposed. Based on the inter-frame difference method, the moving target was identified and the target

area was calculated, then the feature fusion Cam-Shift mean shift algorithm is used to track target. Based on binocular vision, a two-channel parallel target identification and location method was proposed, updating the target three-dimensional information in real time while tracking it. Furthermore, a dynamic collision-free path planning method was implemented, and the minimum distance was derived directly by using the coordinate values of the target in the local coordinate system of the rod. On this basis, the obstacle avoidance gain and escape velocity related to the minimum distance was established, and obstacle avoidance path planning was implemented by using the zero space mapping matrix of redundant robot. Experiments were performed to study the efficiency of the proposed system.

In unknown dynamic environment, the constructed system of dynamic obstacle avoidance path planning for redundant robots has good prospects for the application. But with continuous improvement of the task complexity and the accuracy of the hardware, the requirements for the methods will be higher, and there are a range of issues worthy of further study.

1) The identification and tracking of the dynamic target in the paper does not take into account the uncertainty of the target movement. When the target is partially occluded or produced the rotation deformation, a certain number of feature points will be lost, which is bound to be a great impact on the matching of feature points [28]. Therefore, it should do further research for the situation.

2) Compared to the traditional distance indicators, the pre-selected minimum distance indicators $H_{\text{d-min}}$ optimizes indicators building process, improving the efficiency of dynamic obstacle avoidance. In the future, taking into account that the obstacles will be likely to occur at the end trajectory of the robot, the end pose must be adjusted. How to optimize the global obstacle avoidance path search is a problem that needs further study.

Acknowledgements

The authors would like to thank their colleagues from the Robotics Research Group for helpful discussions and comments on this paper. This work is supported in part by the Key Project of Chinese National Programs for Fundamental Research and Development (973 program) (2013CB73300) and National Natural Science Foundation of China (61573066).

References

1. Flacco F, de Luca A, Khatib O. Control of redundant robots under hard joint constraints: Saturation in the null space. IEEE Transactions on Robotics, 2015, 31(3): 637–654
2. Malysz P, Sirouspour S. A kinematic control framework for single-slave asymmetric teleoperation systems. IEEE Transactions on Robotics, 2011, 27(5): 901–917
3. Xu Z G, Bai X L, Wang J Y, et al. Load carrying capacity test of the space station tedocking manipulator based on the equivalent inertia simulation method. Robot, 2015, 37(2): 231–236
4. Hirano D, Fujii Y, Abiko S, et al. Simultaneous control for end-point motion and vibration suppression of a space robot based on simple dynamic model. Proceedings of the 2014 IEEE International Conference on Robotics and Automation (ICRA'14), May 31–Jun 7, 2014, Hong Kong, China. Piscataway, NJ, USA: IEEE, 2014: 6631–6637
5. Aziminejad A, Tavakoli M, Patel R V, et al. Transparent time-delayed bilateral teleoperation using wave variables. IEEE Transactions on Control Systems Technology, 2008, 16(3): 548–555
6. Lu Y B, Huo X M, Arslan O, et al. Incremental multi-scale search algorithm for dynamic path planning with low worst-case complexity. IEEE Transactions on Systems, Man, and Cybernetics, Part B: Cybernetics, 2011, 41(6): 1556–1570
7. Alise M, Roberts R G, Repperger D W, et al. On extending the wave variable method to multiple-DOF teleoperation systems. IEEE/ASME Transactions on Mechatronics, 2009, 14(1): 55–63
8. Vannoy J, Xiao J. Real-time adaptive motion planning (RAMP) of mobile manipulators in dynamic environments with unforeseen changes. IEEE Transactions on Robotics, 2008, 24(5): 1199–1212
9. Patel R V, Shadpey F, Ranjbaran F, et al. A collision-avoidance scheme for redundant manipulators: Theory and Experiments. Journal of Robotic Systems, 2005, 22(12): 737–757
10. Jan G E, Chang K Y, Parberry I. Optimal path planning for mobile robot navigation. IEEE/ASME Transactions on Mechatronics, 2008, 13(4): 451–460
11. Mabrouk M H, Mclnnes C R. Solving the potential field local minimum problem using internal agent states. Robots and Autonomous Systems, 2008, 56(12): 1050–1060
12. Oriolo G, Ulivi G, Vendittelli M. Real-time map building and navigation for autonomous robots in unknown environments. IEEE Transactions on Systems, Man, and Cybernetics, Part B: Cybernetics, 1998, 28(3): 316–333
13. Tian L F, Collins C. An efficient robot trajectory planning method using a genetic algorithm. Mechatronics, 2004, 14(5): 455–470
14. Secară C, Vlădăreanu L. Iterative strategies for obstacle avoidance of a redundant manipulator. WSEAS Transactions on Mathematics, 2010, 9(3): 211–221
15. Chaoui H, Sicard P, Gueaieb W. ANN-based adaptive control of robotic manipulator with friction and joint eelasticity. IEEE Transactions on Industrial Electronics, 2009, 56(8): 3174–3187
16. Zalama E, Gaudiano P, Coronado L. A real-time, unsupervised neural network for the low-level control of a mobile robot in a nonstationary environment. Neural Networks, 1995, 8(1):103–123
17. Sadeghian H, Villani L, Keshmiri M, et al. Task-space control of robot manipulators with null-space compliance. IEEE Transactions on Robotics, 2014, 30(2): 493–506
18. Sugie T, Fujimoto K, Kito Y. Obstacle avoidance of manipulators with rate constraints. IEEE Transactions on Robotics and Automation, 2003, 19(1): 168–174
19. Jasour A M, Farrokhi M. Path tracking and obstacle avoidance for redundant robotic arms using fuzzy NMPC. Proceedings of the American Control Conference (ACC'09), Jun 10–12, 2009, St. Louis, MO, USA. Piscataway, NJ, USA: IEEE, 2009: 1353–1358

To p. 96

low-pass filter form. Proceedings of the IEEE, 1964, 52(8): 939–963
8. Chen K L, Peroulis D. Design of highly efficient broadband class-E power amplifier using synthesized low-pass matching networks. IEEE Transactions on Microwave Theory and Techniques, 2011, 59(12): 3162–3173

(Editor: Lu Junqiang)

From p. 72

4. Hou X M. A SVM multi classification algorithm for anti-noise speech recognition. Journal of Xi'an University of Posts and Telecommunications, 2009, 14(5):100–105 (in Chinese)
5. Lee Y J, Mangasarian O L. SSVM: A smooth support vector machine for classification. Computational Optimization and Applications, 2001, 20(1): 5–22
6. Yuan Y B, Huang T Z. A polynomial smooth support vector machine for classification. Advanced Data Mining and Applications: Proceedings of the 1st International Conference on Advanced Data Mining and Applications (ADMA'05), Jul 22–24, 2005, Wuhan, China. LNCS 3584. Berlin, Germany: Springer, 2005: 157–164
7. Yuan Y B, Fan W G, Pu D M. Spline function smooth support vector machine for classification. Journal of Industrial and Management Optimization, 2007, 3(3): 529–542
8. Yuan B L, Zhang W J, Wu H. New solution method to smoothing support vector machine with one control parameter smoothing function. Proceedings of the 2nd WRI Global Congress on Intelligent Systems (GCIS'10): Vol 2, Dec 16–17, 2010, Wuhan, China. Piscataway, NJ, USA: IEEE, 2010: 153–156
9. Wu Q, Fan J L. Smooth support vector machine based on piecewise function. The Journal of China Universities of Posts and Telecommunications, 2013, 20(5): 122–128
10. Wu Q, Wang W, Wang L Z. Exponential smooth support vector machine. Journal of Xi'an University of Posts and Telecommunication, 2014, 19(4): 9–14 (in Chinese)
11. Yuan Y K, Byrd R H. Non-quasi-Nowton updates for unconstrained optimization. Journal of Computing Mathematics, 1995, 13(2): 95–107
12. Yuan Y X. A modified BFGS algorithm for unconstrained optimization. IMA Journal of Numerical Analysis, 1991, 11(3): 325–332

(Editor: Lu Junqiang)

From p. 85

20. Yilmaz A, Javed O, Shah M. Object tracking: A survey. ACM Computing Surverys, 2006, 38(4): 1–45
21. Park Y, Lepetit V, Woo W. Extended keyframe detection with stable tracking for multiple 3D object tracking. IEEE Transactions on Visualization and Computer Graphics, 2011, 17(11): 1728–1735
22. de Haan G. Progress in motion estimation for consumer video format conversion. IEEE Transactions on Consumer Electronics, 2000, 46(3): 449–459
23. Chien S Y, Ma S Y, Chen L G. Efficient moving object segmentation algorithm using background registration technique. IEEE Transactions on Circuits and Systems for Video Technology, 2002, 12(7): 577–585
24. Tsalatsanis A, Valavanis K, Yalcin A. Vision based target tracking and collision avoidance for mobile robots. Journal of Intelligent and Robotic Systems, 2007, 48(2): 285–304
25. Gao X, Hu H, Jia Q X, et al. 3-D augmented reality teleoperated robot system based on dual vision. The Journal of China Universties of Posts and Telecommunications, 2011, 18(1): 105–112
26. Jia Q X, Zhang Q R, Gao X, et al. Dynamic obstacle avoidance algorithm for redundant robot with pre-selected minimum distance index. Robot, 2013, 35(1): 17–22 (in Chinese)
27. Fragkopoulos C, Graser A. Dynamic efficient collision checking method of robot arm paths in configuration space. Proceedings of the IEEE/ASME International Conference on Advanced Intelligent Mechatronics (AIM'11), Jul 3–7, 2011, Budapest, Hungary. Piscataway, NJ, USA: IEEE, 2011: 784–789
28. Gao X, Jia Q X, Sun H X, et al. A multi-layer occlusion handling method based on stereo vision and pose estimation for real-time augmented reality. Journal of Information and Computational Science, 2010, 7 (12): 2548–2555

(Editor: Lu Junqiang)